Journal of
Low Power Electronics and Applications

MDPI

Article

Ultra-Low Power Consuming Direct Radiation Sensors Based on Floating Gate Structures

Evgeny Pikhay [1,2,*], Yakov Roizin [1,2] and Yael Nemirovsky [2]

[1] TowerJazz, 2310520 Migdal HaEmek, Israel; yakovro@towersemi.com
[2] Technion-Israel Institute of Technology, Technion City, 32000 Haifa, Israel; nemirov@ee.technion.ac.il
* Correspondence: evgenypi@towersemi.com; Tel.: +972-4650-6645

Received: 21 June 2017; Accepted: 28 July 2017; Published: 31 July 2017

Abstract: In this paper, we report on ultra-low power consuming single poly floating gate direct radiation sensors. The developed devices are intended for total ionizing dose (TID) measurements and fabricated in a standard CMOS process flow. Sensor design and operation is discussed in detail. Original array sensors were suggested and fabricated that allowed high statistical significance of the radiation measurements and radiation imaging functions. Single sensors and array sensors were analyzed in combination with the specially developed test structures. This allowed insight into the physics of sensor operations and exclusion of the phenomena related to material degradation under irradiation in the interpretation of the measurement results. Response of the developed sensors to various sources of ionizing radiation (Gamma, X-ray, UV, energetic ions) was investigated. The optimal design of sensor for implementation in dosimetry systems was suggested. The roadmap for future improvement of sensor performance is suggested.

Keywords: radiation sensor; floating gate; CMOS; semiconductor; energetic ions; Gamma; X-ray; UV

1. Introduction

Characterization of ionizing radiation is required in numerous applications related to safety, medicine, defense, industry and research. It is necessary to measure radiation doses in a broad range starting from the level of few microGy in safety and medical imaging applications, of the order of few Gy in radiotherapy treatments and up to several hundreds of kGy in Gamma and X-ray sterilization. Various types of dosimetry systems, operating on different physical principles are known. Most of them suffer of such drawbacks as high cost, bulky dimensions, complex and time consuming read-out, etc. Meantime, the emerging approaches, like IoT, require compact, cheap, ultra-low power consuming sensors that could be used in precise CMOS SoC dosimeters and would allow fast and easy read-out. Despite numerous researches in the field, limited data on low power radiation sensors was published. The issues related to physics of operation and degradation phenomena under irradiation for low power sensing systems require in-depth studies. This is especially important for scaled down sensors fabricated in advanced semiconductor technologies.

1.1. Radiation Sensing Techniques in CMOS Technology

Three well known types of direct semiconductor radiation sensors are based on: (i) diode leakage [1–3]; (ii) capacitor discharge [4]; and (iii) MOS transistor degradation [5–9].

In the first case, the PIN diode is operated at high reverse bias, and the leakage current is monitored. The ionizing agent (charged particle or photon) creates charge in the depletion region and contributes to the leakage current. The increase in leakage current is detected by the external circuitry, analyzed and then a conclusion on the ionizing agent parameters (energy, dose, etc.) can be made. The high volume of diode intrinsic region is required to increase the sensitivity of the diode-type sensor.

The operation of capacitor-type sensor is also based on collection of charge produced by ionizing agent, but the method is different. The capacitor is charged before the exposure, and the charge, created by ionizing agent in capacitor dielectric, is separated by electric field and drifts to capacitor plates, leading to gradual discharge of capacitor. As a result, the capacitor voltage decreases and the information about radiation influence can be obtained.

Another type of semiconductor radiation sensors utilizes the degradation of MOS transistor dielectric, caused by ionizing radiation. The radiation creates traps (dangling bonds) in Silicon Oxide, which can be occupied by charges. This, in turn, leads to changes in Drain-Source current of the transistor, which can be detected by external circuitry. The drawback of this sensor type is that the trapped charges are not stable: they can de-trap and sensor readings will change unrelated to radiation.

In case of diode-based and capacitor-based sensors, the material degradation is also present and can introduce peculiarities in sensors readings. However, these devices can be engineered to minimize and precisely estimate degradation, so that correction schemes can be introduced to significantly reduce its influence. On the contrary, the transistor-type sensor is based solely on degradation. Since 100% of its signal comes from degradation, the performance of the sensor depends on its thermal history (annealing). Thus, the mistakes in dose estimation can be higher than in case of diode and capacitor, where only part of signal comes from degradation.

One of the ways to utilize capacitor principle for building radiation sensor is to use floating gate (FG) non-volatile memory (NVM) device, which includes two or more coupled capacitors. The floating gate represents one of the capacitor plates. The FG is charged before the exposure and discharged by radiation. The radiation information can be extracted by measuring the current variation in the NVM device.

Various types of FG NVM devices exist. For example, we will consider FG NVM memory cell based on NMOS transistor. When FG is introduced into NMOS gate dielectric (Figure 1a), the gate becomes "Control Gate" (CG) to distinguish it from FG. Introducing FG allows to adjust Vt (i.e., to shift Id-Vg curve) by storing electrons or holes in the FG. Charging of the FG is done by Fowler-Nordheim tunneling or one of hot carriers injection mechanisms.

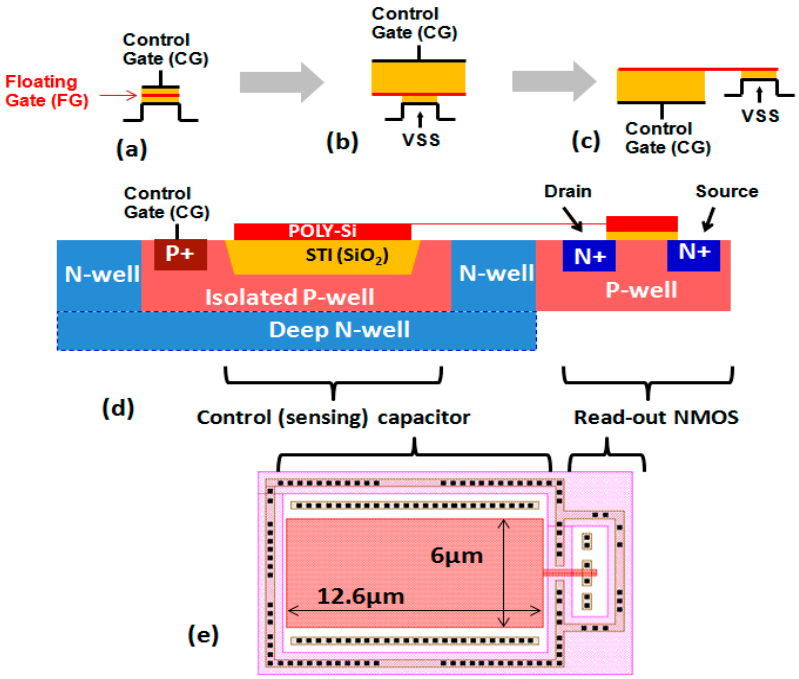

Figure 1. Radiation sensor in CMOS technology: (**a**) standard FG NVM cell; (**b**) FG NVM cell modified to enhance sensitivity to radiation; (**c**,**d**) schematic implementation of sensor in CMOS technology; (**e**) radiation sensor layout (some layers are omitted).

Like in the described above capacitor-type radiation sensor, the FG NVM cell will be discharged by ionizing radiation. Detectors of ionizing radiation, based on of-the-shelf NVM products were proposed in [10–12]. The FGs of the NVM devices are charged before the exposure, and read failures during irradiation are used for the estimation of the absorbed dose. The dose resolution is typically low, because the volume of sensing devices is small.

1.2. C-Sensor Principle, Structure and Operation

In this work, we used TowerJazz embedded NVMs [13–15], for measuring the total dose (TID) of ionizing radiation. The design of memory cells was modified to enhance the response to radiation (Figure 1a,b). For this purpose, the control capacitor residing in NVM cells on gate oxide was formed using the STI dielectric (Figure 1c) with the thickness of 3500 A, which is more than 30 times higher than gate oxide thickness (110 A in 5 V CMOS technology). Charge injection into the FG of radiation sensors is performed by Fowler-Nordheim mechanism: high voltage is applied between the Isolated P-well and the substrate (of NMOS). The developed radiation sensor comprises the features of single Poly NVM devices specially developed for ultra-low power applications [13]. It requires less than 1uW per cell for programming (i.e., charging of the FG). Thus, sensor can be implemented in IoT systems, such as battery-less RFID SoC [14].

The important characteristic of the radiation sensor is its coupling ratio (CR)—the relation between the control capacitor (STI) and read-out capacitor (GOX) values. A high coupling ratio (above 10) ensures high gm of the read-out NMOS (close to that of standard NMOS) and allows to minimize the injection voltages (the applied voltages falls on the GOX between the FG and the substrate). The layout of one of the developed sensor with minimum Design Rule (DR) NMOS and CR = 10 is shown in Figure 1e. Id-Vg characteristics for different amount of charge in FG (readout mode) are presented in Figure 2a. The charging/discharging curves of the sensor are shown in Figure 2b.

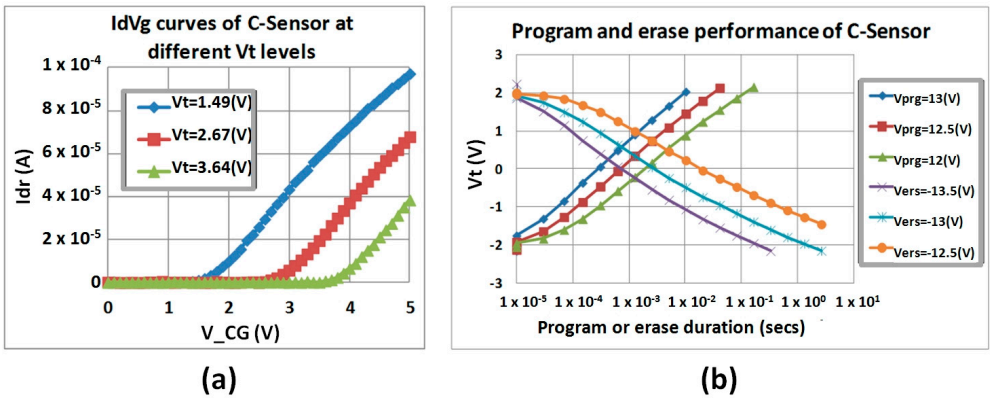

Figure 2. Operation of radiation sensor: (**a**) Id-Vcg curves for different amount of charge in FG; (**b**) charging/discharging curves (Vt vs. pulse duration).

The sensor in Figure 1 can be utilized in practical applications, but has limitations, similar to other semiconductor sensor solutions [16–25]:

1. The F-N injection occurs in the read-out NMOS transistor. The injection takes place in high electric fields and may cause damage to GOX by introducing charged traps. This charge is not stable, leading to Vt instabilities.
2. The sensor requires very high voltages for charge injection into the FG, typically 12–14 V (110 A GOX). These voltages cannot be supplied using the main CMOS platform transistors (5 V), so that special high voltage devices are required to facilitate switching.

3. Even if special high-voltage devices were fabricated in a certain CMOS process flavor, to select a sensor for charging in case when sensors are arranged in 2D array, HV devices have to be introduced into each cell.

An advanced sensor device designed and fabricated to overcome the mentioned limitations is called "C-Sensor" (C stands for "complimentary"), to link it with its NVM prototype with a CMOS inverter in the readout circuit. A tunneling capacitor residing in an isolated p-well was introduced into the sensor design (Figure 3). One plate of this capacitor is represented by the FG, shared with other components of sensor (control capacitor and read-out transistor). Another plate is the mentioned isolated P-well. This additional isolated P-well is called Tunneling Gate (TG). Gate dielectric of Tunneling Capacitor is GOX.

The programming is still performed by Fowler-Nordheim tunneling, but the voltage is applied in a different way: −5 V is applied to Tunneling Gate (TG) and 7–9 V is applied to the Control Gate (CG). The coupling ratio between Control capacitor and Tunneling capacitor is 10, so that 90% of applied voltage falls on GOX of the Tunneling Capacitor, and the F-N tunneling of electrons occurs in Tunneling capacitor, and not in Read-out NMOS (as in the device of Figure 1). Therefore, only the Tunneling capacitor is under high voltage, while only a part of the applied voltage falls on the GOX of NMOS. This prevents the GOX of the readout NMOS from degradation. The detrapping of charge, as explained above, occurs in Tunneling capacitor, and its influence on Vt stability is much weaker (more than 10 times from the electrostatic considerations).

Sharing of charging voltage between TG and CG also allows to resolve the mentioned above issues (1) and (2). Standard CMOS platform transistors in cascade connection can be utilized for switching the voltages in the range ± 9 V, thus eliminating the need for special high-voltage devices. Drawing TG and CG lines orthogonally in 2D matrix of sensors allow selecting a single sensor for charging, by TG and CG in a cross-wise configuration.

To allow additional flexibility in sensor read-out and in the design of the dosimetry system, the PMOS read-out transistor was introduced into sensor design (Figure 3). Thus, the sensor read-out can be performed in various ways, e.g., by reading from NMOS or PMOS, or using both transistor currents, or switching both transistors as a CMOS inverter and performing logic readout of voltage. Therefore, the sensor can be used in dosimetry systems of different designs without a need to modify the sensor. For example, the reading scheme with PMOS transistor has advantage of improved radiation hardness, comparing to NMOS, as explained in Section 3.2 below.

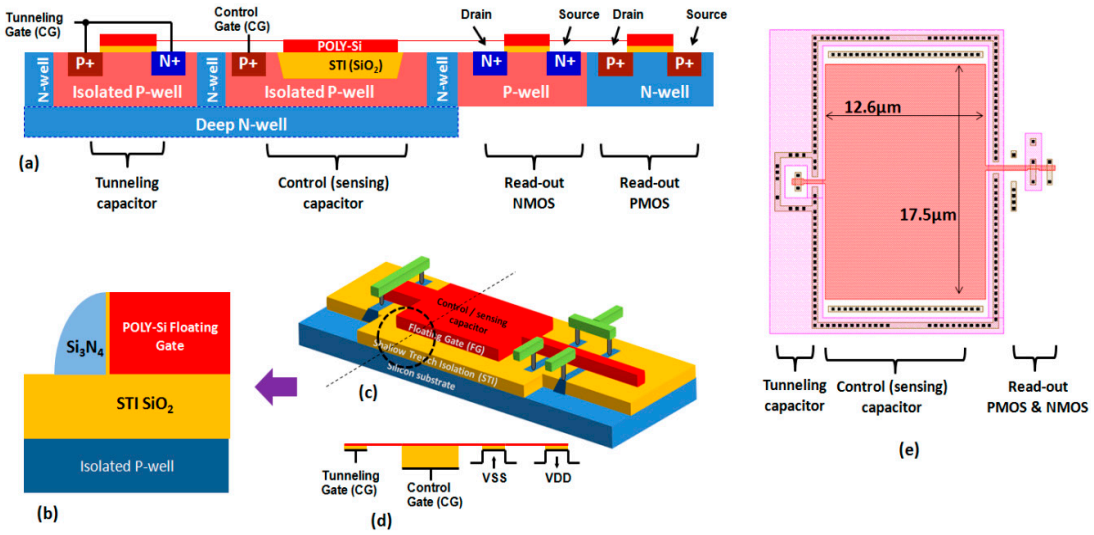

Figure 3. Advanced version of C-Sensor cell, utilized in practical systems design: (**a**) schematic cross-section; (**b**) dielectrics surrounding FG; (**c**) schematic 3D view; (**d**) principal electrical scheme; (**e**) layout (some layers are omitted).

1.3. Brief Review of Physical Mechanisms Involved in Sensor Operation

The process of radiation detection by C-Sensor consists of two steps. First, the incident radiation generates energetic charges in C-Sensor volume (both in semiconductor and dielectric regions). Second, the produced electrons and holes can charge or discharge the FG. Any change in the amount of charge in the FG of C-Sensor leads to Vt change, which, in turn, can be detected/amplified by an external electrical circuit.

Various mechanisms of primary radiation-matter interactions are known [26,27]. Among them, Photoelectric effect and Compton scattering are relevant for C-Sensor operation, due to the energy range of particles in practical applications (from few keV to few MeV) and sensor material (Silicon). The charges, generated in the mentioned mechanisms, can discharge the C-Sensor FG by two possible scenari [28–30] (Figure 4):

1. "Emission". Energetic electrons may transfer a part of their energy (directly or by secondary electrons or holes) to the charges in the FG (Polysilicon) or/and in the substrate. The transferred energy is sufficient for the electrons to overcome the oxide potential barrier, which leads to the discharge of the FG.
2. "Separation". The e-h pairs produced in the dielectric (STI) are separated in the electric field in this dielectric. Some of the electrons and holes reach the FG and discharge it.

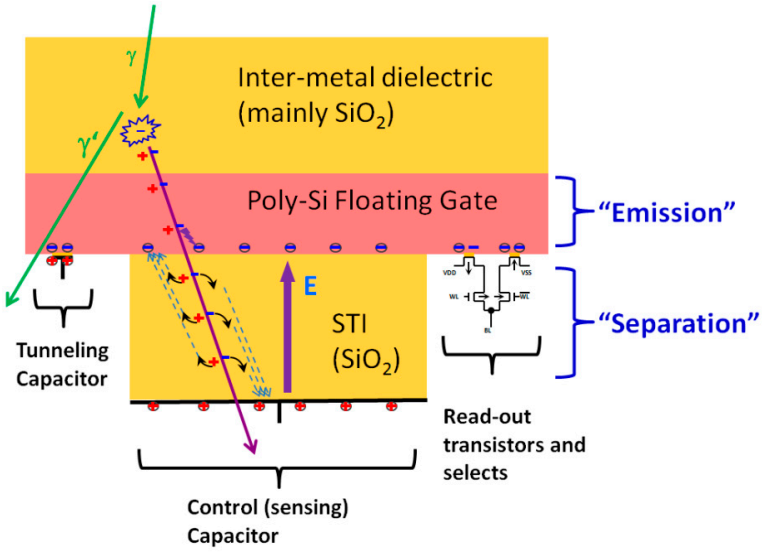

Figure 4. Illustration of C-Sensor discharge mechanisms.

Since each of the two above mentioned mechanisms ("emission" and "separation") is associated with different part of C-Sensor—namely, Poly and STI—we investigated the contribution of each mechanism by modifying the cell design and studying the response to different types of radiation.

2. Methods and Devices

With the aim to reveal the contribution of each involved physical mechanism, we prepared different types of special test structures and devices and exposed them to different types of radiation.

The prepared structures are divided into three types:

1. Single sensors.
2. MOS transistors.
3. Array sensors.

Different types of single sensors (Section 2.1 below) serve for investigation of discharge mechanism. MOS transistor structures (Section 2.2 below) were utilized to study sensor degradation. Array sensors (Section 2.3 below) are intended for statistical analysis of single sensor behavior and for demonstrating the capabilities of the suggested sensors for Gamma and X-ray direct imaging.

Three types of radiation were systematically employed in the performed experiments: Gamma, X-ray and UV. They differ by photon energy and, consequently, by dominating mechanism of interaction with the sensor. Exposing the corresponding types of sensors and transistor structures to different types of radiation allowed to make conclusions about mechanisms responsible for discharge and degradation of sensor, and finally, allowed to provide guidelines for sensor improvement.

2.1. Single Sensors

C-Sensors having different Poly electrode shapes and different doping of sensing capacitor plates (Poly and Silicon) were prepared to investigate sensor discharge mechanism, as summarized in Figure 5. These structures were developed to compare the contribution of "emission" and "separation" mechanisms (defined in Introduction), when C-Sensor was exposed to different types of radiation. In "emission" mechanism, the electrons stored in FG are emitted from the entire surface (lateral and vertical walls of Poly), while in "separation", mainly the lateral area of Poly, facing the silicon substrate surface, defines the discharge rate. The doping of Poly and Silicon in the region of sensing capacitor may influence C-Sensor performance for both "emission" and "separation" mechanisms. For example, emission of electrons from charged Poly or substrate depends on the material work function. Doping of Poly was performed using the masks from the core CMOS process flow, for example, N+/P+ implants used in the core CMOS for source/drain formation of NMOS and PMOS transistors. Doping of Si (second plate of control capacitor) was done by using N-well and P-well implants from the core CMOS process flow.

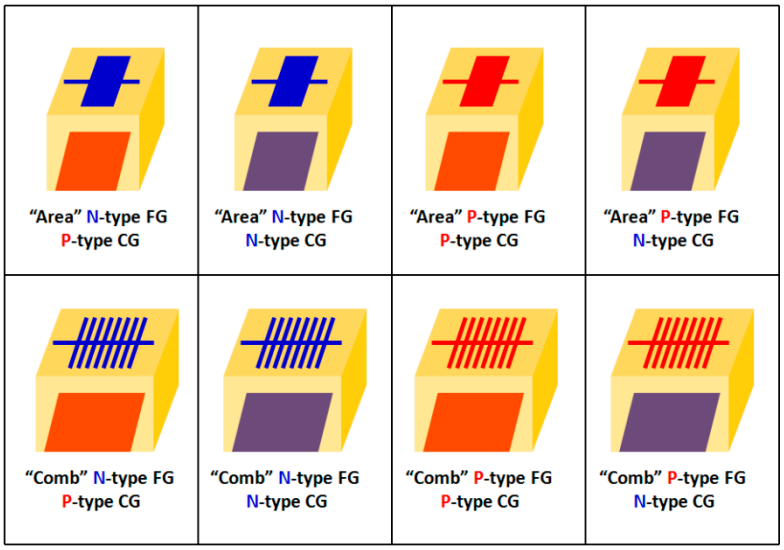

Figure 5. Different types of C-Sensors for discharge mechanism investigation.

2.2. MOS Transistors

The C-Sensor FG is surrounded by relatively thick dielectrics: STIthickness is 3000–3500 A; Si_3N_4 spacerwidth is about 1000 A (Figure 3b). The ionizing radiation produces electrical charges, which can be trapped in these dielectrics [31,32]. This, in turn, influences various sensor parameters. For example, holes trapped in the STI may influence the sensor readings. Also, these holes can be emitted from traps, leading to readout instabilities.

The common practice in assessing the sensor radiation immunity is performing multiple irradiations that require plenty of time and resources. Below, we describe an alternative approach that employed the developed test structures with the same dielectrics isolating the FG in real C-Sensors. These structures allow direct measurements of the electric charge trapped in the insulators surrounding the FG as a result of irradiation.

The first two types of structures are NMOS transistors with Polysilicon gate and N-well drain and source: one with P-well substrate and another native (not implanted silicon) p-type, 1–2 Ohm*cm substrate (Figure 6a). Typical Id-Vg curves of these devices correspond to threshold voltages of about 35 V and 0 V for P-well and native transistors. The value of Vt is high due to thick STI dielectric (3500 A) serving as the gate oxide and relatively high P-well doping (above 1E17 cm^{-3}). The estimated initial surface charge is below 1E11 cm^{-2}. Vt was measured at Id = 1 μA.

The second two types of structures are PMOS transistors with Polysilicon gate and P-well drain and source: one with N-well substrate and another with the native substrate (Figure 6b). The N-well substrate is implemented using N-well and deep N-well implants of a standard CMOS process. Id-Vg curves show threshold voltages of about −40 V and −5 V for N-well and native transistors, correspondingly.

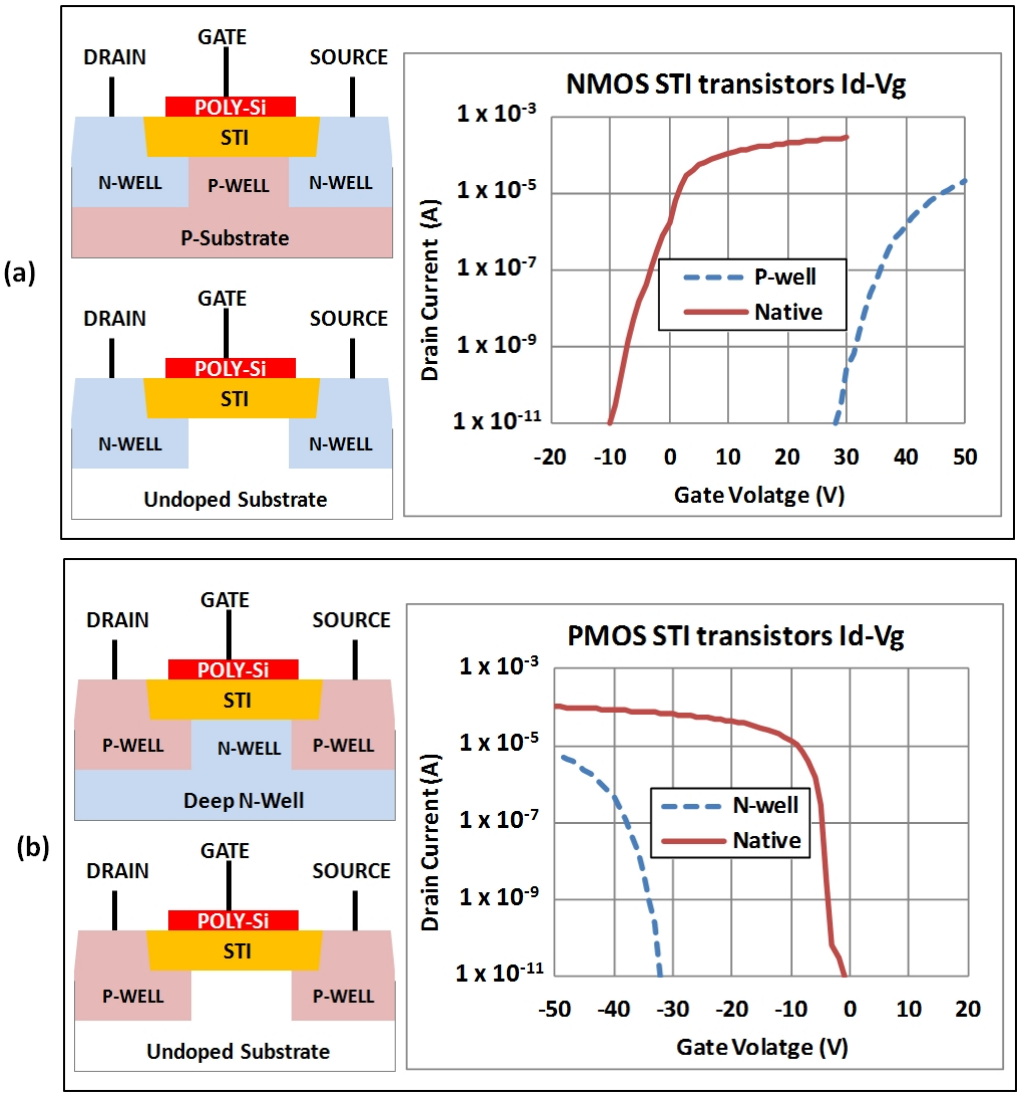

Figure 6. *Cont.*

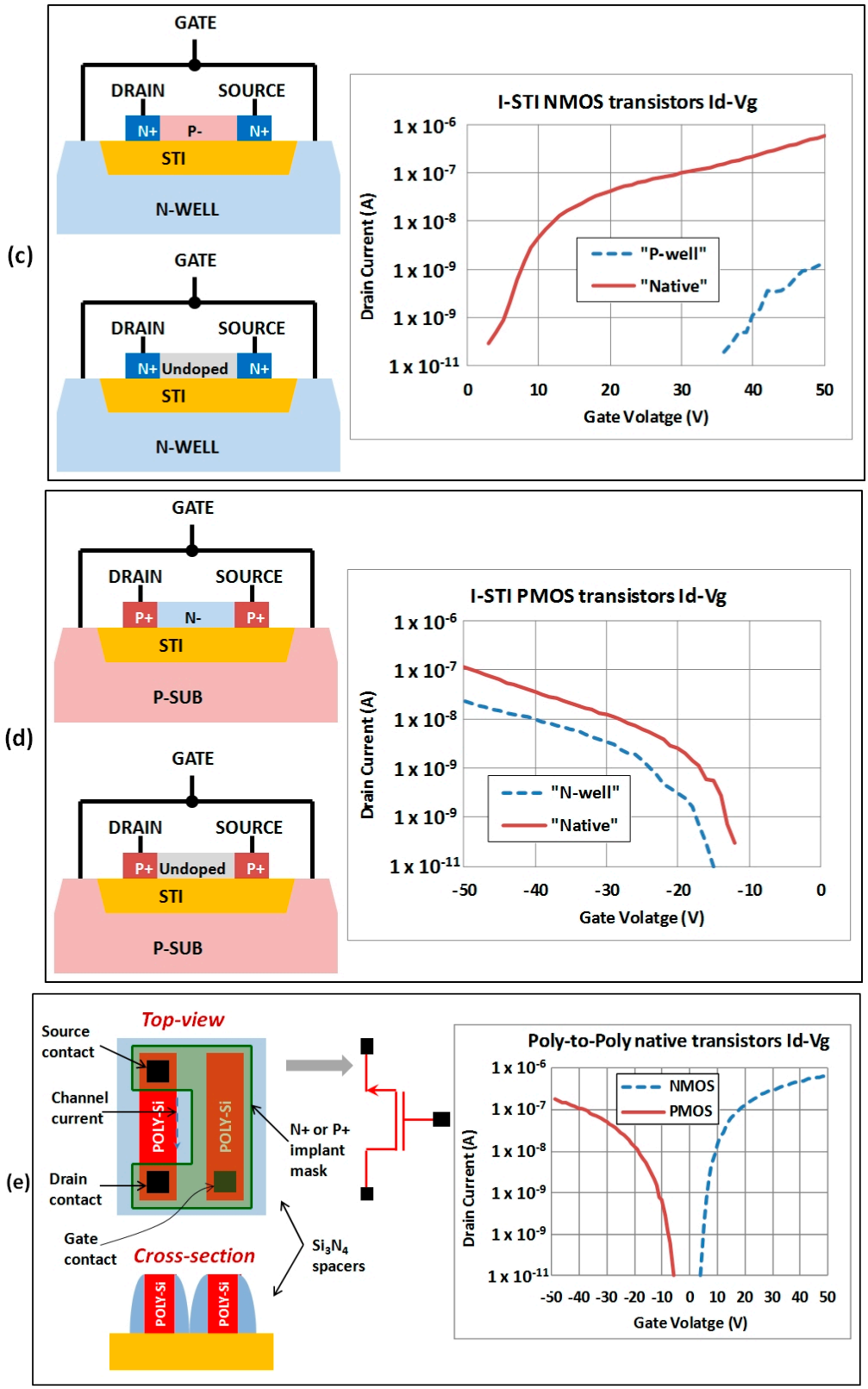

Figure 6. Special MOS structures with corresponding Id-Vg curves: (**a**) NMOS; (**b**) PMOS; (**c**) Inverse NMOS; (**d**) Inverse PMOS; (**e**) Poly-to-Poly.

The third two types of test-structures are "inversed" STI (I-STI) NMOS transistors, where the Poly plays the role of a "substrate", and P-well of standard CMOS plays the role of "Gate". The drain and source are represented by N+ implants in Poly (Figure 6c). The "P-well" is implemented by doping the channel region of Poly by P-LDD implant ("lightly doped drain" extensions of standard CMOS technology). The native device is implemented by leaving the channel region of Poly undoped.

The mobility of charge carriers in Poly is many orders of magnitude lower than in crystalline Silicon. Therefore, the drain current of "inversed" STI transistors is much lower than in the case of "conventional" STI transistors. In addition, the difference between "native" and "P-well" I-STI transistors is larger than in the "conventional" STI case, because the dose of P-LDD implant utilized to form the "P-well" of the I-STI NMOS is ~20 times higher than the dose of the standard P-well.

I-STI PMOS transistors similar to I-STI NMOS mentioned above are the fourth group of transistor test-structures. The drain and source are formed by P+ implants in Poly (Figure 6d). The "N-well" is implemented by doping the channel region of Poly with N-LDD implant. "Native" devices are implemented by leaving the channel region of Poly undoped.

The fifth group of devices is Poly-to-Poly transistors consisting of two Poly bars, one of them heavily doped and playing the role of a gate, while the other plays the role of substrate (channel at the sidewall of the Poly bar). The doped regions at the edges act as drain and source terminals (Figure 6e). There are two Poly-to-Poly structures, one with N+ gate and S/D diffusions and one with P+ gate and S/D diffusions.

In order to study the built-up of charge in dielectrics surrounding the FG, the described above test structures were subjected to different doses of Gamma radiation (Co-60 source, dose rate 0.85 Gy/h) in a passive mode. Id-Vg curves were measured before and after the exposure. Measurements results and analysis are presented in Section 3.2.

2.3. Array Sensors

In order to perform the statistical study of C-Sensors, an array of 4096 (4k) C-sensors was built. It allowed to perform simultaneous pre-charge of all 4k sensors in the array, and random access to each sensor for the readout. The readout of individual sensors in the array is performed using a CMOS inverter principle. The charge stored in the FG corresponds to the shift in Vm (mid-point inverter voltage). The state of all sensors in the array is represented by Vm distribution (Section 3.3).

3. Experimental Results

3.1. Single Sensors Results

Typical discharge kinetics of the C-Sensor exposed to Gamma rays is presented in Figure 7. The C-Sensor was pre-charged to Vt = 4 V and exposed to the radiation beam from a medical linear accelerator CLINAC 700C (Varian). The minimal and peak energy of photons are 2 MeV and 5 MeV respectively. The Vt of sensor was measured after exposure to different absorbed doses (5 Gy, 10 Gy, 20 Gy, 50 Gy, 100 Gy and 150 Gy).

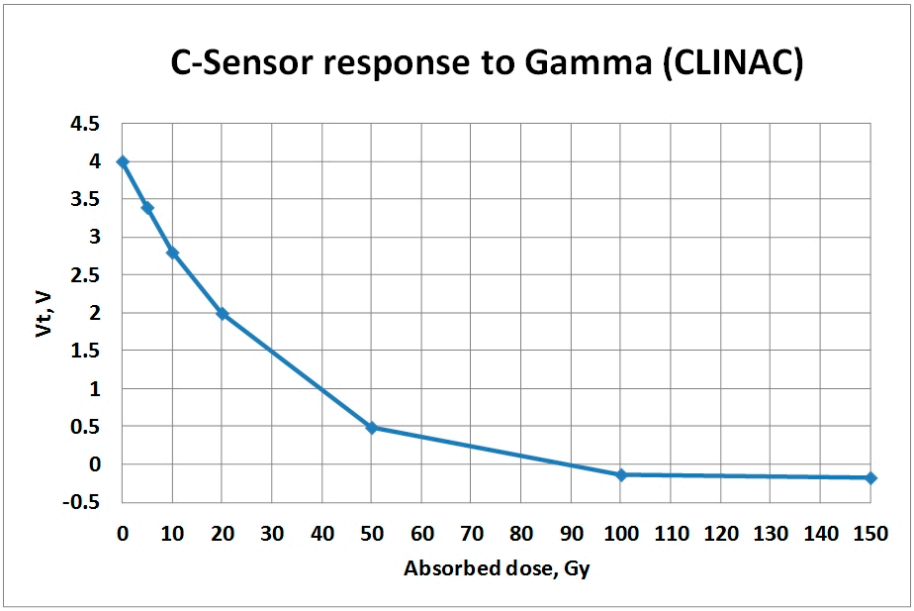

Figure 7. Typical kinetics of C-Sensor discharge.

As seen from Figure 7, at the beginning of discharge the Vt loss is nearly linear. In this mode the sensor is supposed to operate in the products. For doses above 100 Gy, Vt of sensor saturates. In this research, we investigated the behavior of different sensors flavors (different geometries and doping of the FG and CG plates) in "linear" and "saturation" stages of FG discharge (the parentheses with "linear" and "saturation" are used to avoid confusion with linear and saturation modes of MOS transistor operation).

This section describes the results of irradiation of C-Sensors having different shapes of FG ("comb" vs. "area") and different doping of FG and CG (Figure 5) by UV (254 nm) and Gamma (Co-60) sources. The intensity of the UV source is at the level of ~5 mW/cm^2. The dose rate of Co-60 source was about 0.9 Gy/min.

The aim of experiments described in this section is to define the dominating mechanism of sensor discharge by ionizing radiation: "emission" or "separation".

The method is based on the comparison of C-Sensors response to UV and Gamma radiation. In the case of UV, the discharge mechanism is "emission" [33], since the photon energy of a mercury lamp is below 5 eV and the SiO_2 band-gap is above 9 eV.

All sensors were charged to the same Vt level of ~3 V before irradiations. The first group of sensors of all geometries and dopings (Figure 5) was exposed to UV. The second group of sensors was irradiated with Gamma. The behavior of sensors of different kinds is analyzed below for both types of radiation.

The response of sensors to UV is summarized in Figure 8a ("linear" stage of discharge, Vt shift for the same exposure time) and in Figure 8b (Vt level at "saturation" stage of discharge).

1. "Linear" stage (UV irradiation):

    a. Impact of the periphery length (same FG footprint area): sensors with larger FG periphery ("Comb-FG") showed higher discharge rate. This corresponds to a model where the FG discharge occurs by emission of electrons from the FG in contact with the STI where adsorption of UV photons takes place.
    b. Impact of doping: sensors with larger work function difference between FG to CG (with an account of the sign of this difference) showed higher discharge rate (Figure 8a). This observation is explained by two physical peculiarities. First, larger work function

difference (between CG and FG) leads to higher electric field enhancing the flow rate of electrons from FG to CG. Secondly, the results suggest that dominating flow of electrons from the negatively charged FG is from the valence band, and not the conduction band. For example, the FG discharge rate is higher in the case of P+ to N− structure, even though the emission for N+ to P− could be assumed to happen from the conduction band of the strongly doped N+ FG.

2. "Saturation" stage (UV irradiation):

   a. Impact of periphery length: the level of Vt saturation does not depend on periphery length. As was already mentioned in Introduction, the discharge kinetics of the FG discharge is connected with the balance of electrons flowing to and from the FG. The final FG charge depends on the electric field distribution, but not on the periphery length, which defines the FG charge decay kinetics.

   b. Impact of doping: the saturation level decreases as the work function difference between FG and CG decreases. This can be explained by the following mechanism: The intrinsic Vt of the readout transistor depends on the doping of substrate and the FG above it. In our layout, the FG doping over the readout transistor is always N+. The measured Vt of the C-sensor corresponds to a device with charged FG and can be both higher and lower than the intrinsic Vt, depending on the sign of charge in the FG. Let us consider, e.g., a situation when the FG in the control capacitor area is P+ and the opposite electrode (CG) is N−. In this case, there is an electric field in STI under the FG control capacitor area with lines of force starting at CG and terminating at the FG. Under irradiation, the mentioned field will result in continuous separation of the electrons and holes excited by the UV radiation. The electric field decreases to very small values, which corresponds to charging of the FG with positive charge. Actually, the voltage corresponding to this charging is ~0.7–0.8 V (difference between the Fermi levels of P+ and N− silicon). This voltage is connected in series with the gate of the read-out transistor and decreases its effective Vt by ~0.8 V. It is clear that with N+ to P− combination, the generated by radiation voltage will be opposite, and Vt would increase by ~0.7–0.8 V. These considerations explain the observed in Figure 8b ~1.5–1.6 V variation for the fabricated test-structures after prolonged irradiation with UV.

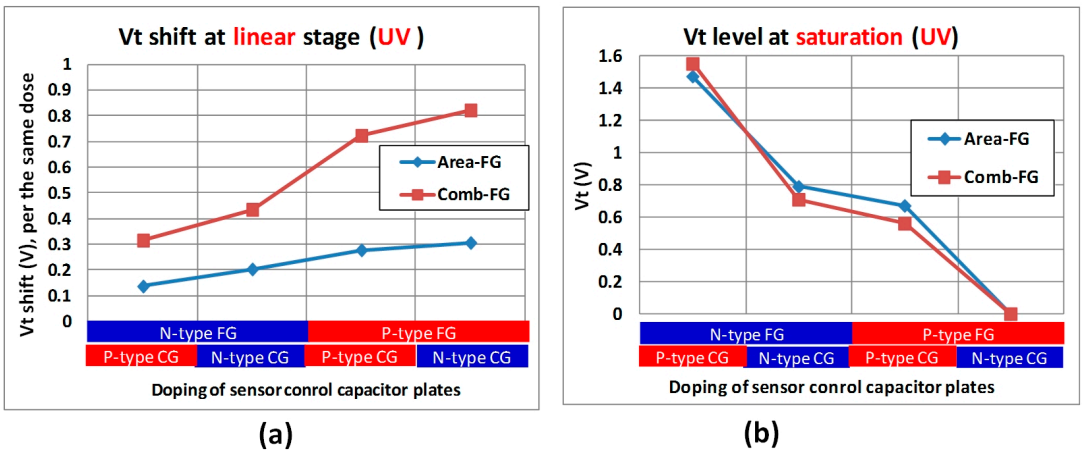

Figure 8. The summary of UV irradiations of structures described in Figure 5: (**a**) "linear" and (**b**) "saturation" stages.

Another group of sensors was pre-charged to the same level of 3 V and exposed to doses of 10 Gy and 20 Gy ("linear" response) and 500 Gy and 1000 Gy ("saturation"). The response of sensors in "linear" (Figure 9a) and "saturation" (Figure 6b) stages of discharge are analyzed similar as in the case

of UV irradiation: for "linear" stage, the Vt loss is compared, for "saturation" stage, the final Vt levels are compared.

1. "Linear" stage (Gamma irradiation):

    a. Impact of periphery length: the discharge rate in "area-FG" case is higher than in "Comb-FG" case, for all combinations of FG and CG doping. This indicates, first, that edge fields at Poly fingers are not critical in the discharge mechanism. The vertical field under the charged continuous FG in corresponding specimens is higher than for finger type counterparts. Increasing the periphery length of FG did not result in faster discharge. Thus, "separation" mechanism dominates over "emission" mechanism. It is worth mentioning that it could be expected that more sparse Poly fingers would result in increased sensitivity. Nevertheless, such effect was not observed, and even a certain sensitivity decrease was registered. This leads to a conclusion that reduction of STI thickness in "area" type C-Sensor could provide an improvement in its response to radiation.

    b. Impact of doping: the systematic dependence of discharge rate on doping of CG and FG is observed, mainly in "area-FG" structures: faster discharge corresponds to higher difference between Conduction (or Valence) band energy level of CG and FG (arrow "A" in Figure 10): for higher EC,CG-EC,FG (or EV,CG-EC,FG), the higher response is observed. The weaker dependence on doping in "comb-FG" structures can be explained by lower electrical fields.

2. "Saturation" stage (Gamma irradiation): no dependence of Vt level on FG shape was observed: "comb" and "area" type sensors reached the same level of Vt after continuous discharge. The explanation of this result is similar to the case of UV irradiation. In the case of Gamma rays, electrons and holes can be created inside STI or diffused from the adjacent solid state areas into the STI. Nevertheless, the final state of the system is the same, since the discharge continues up to the stage when the electric field in the control capacitor becomes very small.

In summary, we conclude that electrical field effects ("separation" mechanism) dominate in the kinetics of the GG discharge in the "linear" Vt decrease region. It also follows from these results that there could be an optimum STI thickness for achieving high sensitivity (lower volume but higher electrical field).

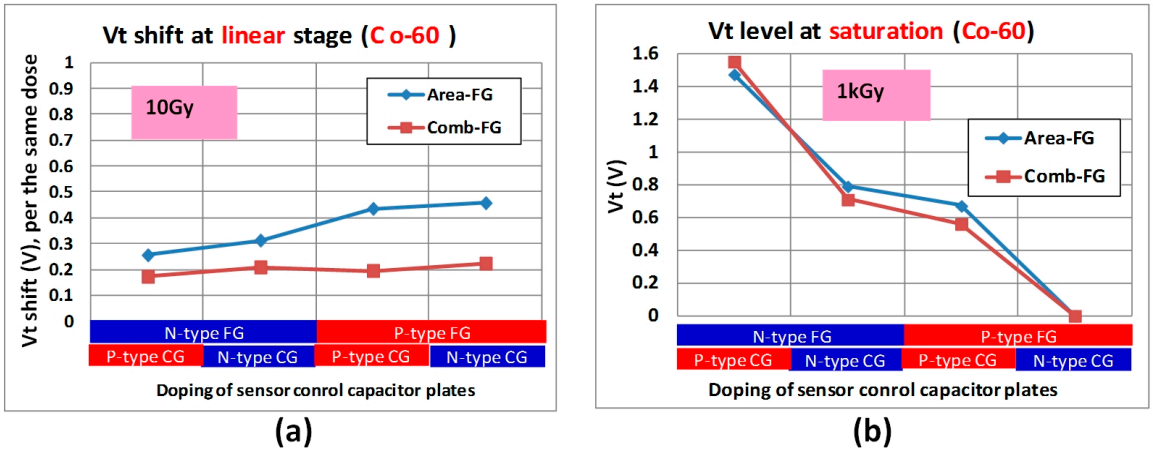

Figure 9. The summary of Co-60 irradiations of structures described in Figure 5: (**a**) "linear" and (**b**) "saturation" stages.

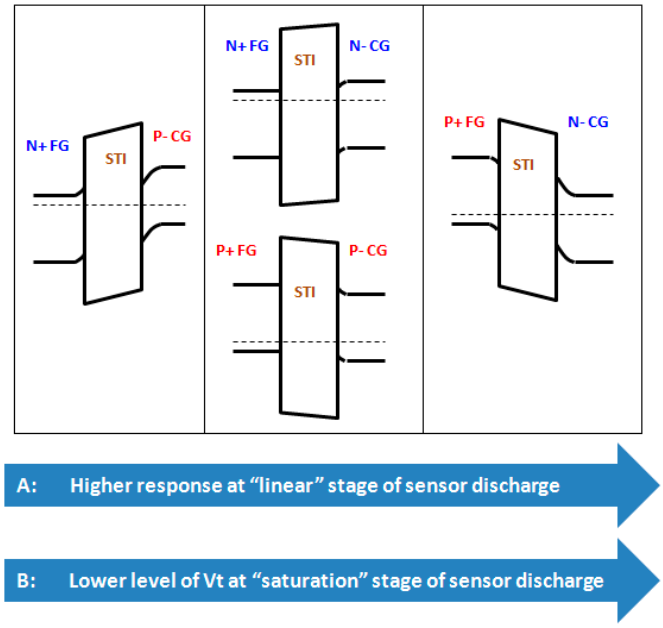

Figure 10. Band diagram of sensing capacitor for different combinations of FG (Poly plate) and CG (Si plate) doping.

3.2. MOS Structures Results

In order to study the built-up of charge in dielectrics, the test structures described in Section 2.2 above were exposed to different doses of Gamma radiation (Co-60 source, dose rate 0.85 Gy/h) in a passive mode. Id-Vg curves were measured before and after the exposure. To account for the spread of the measured Vt change (before and after irradiation) for each test case, average values of Vt change were calculated. The analysis of the obtained results is summarized in Figure 11.

In Figure 11, we see that NMOS STI transistor with P-well substrate shows significantly higher Vt change than the rest of the devices, in particular vs. identical transistors with undoped substrate. The difference is attributed to P-well doping.

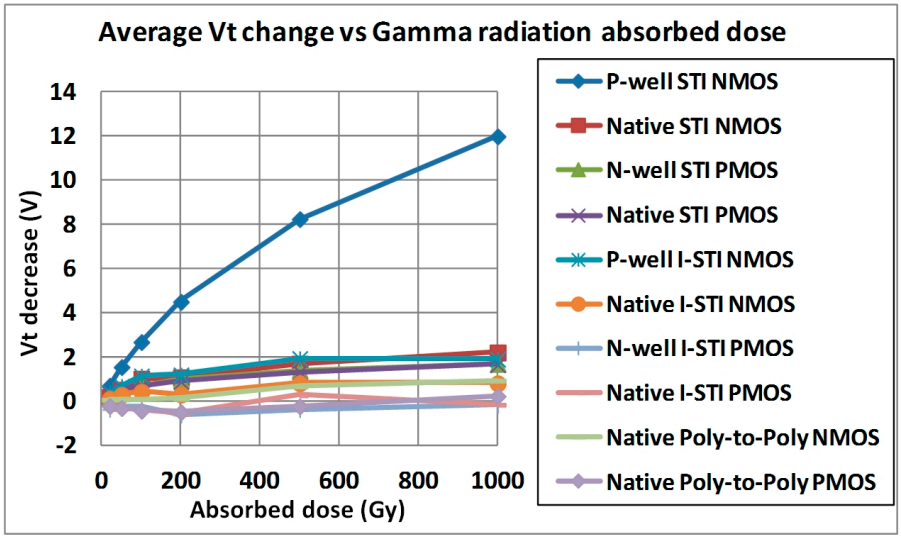

Figure 11. The average Vt change vs. Gamma radiation absorbed dose for all types of tested structures. All the data is normalized so that positive Vt changes correspond to positive trapped charge in the dielectrics. Each data point corresponds to an average of 10 measured transistors.

The observed built-up of positive charge at Si/SiO_2 interface of MOS structures due to the exposure to ionizing radiation is in agreement with published results, see, e.g., [34]. Out of all studied test structures, NMOS STI transistors had poor radiation immunity. NMOS STI radiation immunity improved to the level of other test structures when Boron body implant was skipped. Similar to [35], we argue that this may be connected with the deactivation of Boron implant in Si substrate by Hydrogen released from Si/SiO_2 interface by the ionizing radiation.

Skipping of the Boron implant in the bulk of STI devices, identical to the sensing region of the C-Sensor, resulted in the increased radiation immunity. This significantly broadens the range of measured radiation doses because the floating gate could be programmed and discharged by radiation much more times without device degradation.

3.3. Array Sensors Results

The irradiation experiments with arrays were performed in a way similar to the single cells: the arrays were pre-charged, irradiated by different doses, and Vt distributions before and after exposure were recorded (Figure 12).

As in the case of single cells, we observe a nearly linear response of Vm in the range of low doses of the order of single Grays: ~100 mV for 1 Gy. For higher doses (tens of Grays), the sensitivity decreases to ~85 mV for 1 Gy. The sensor is completely discharged by 150 Gy.

Another important observation from the array irradiation experiments is excellent cell-to-cell repeatability, which is confirmed by tight Vm distributions for all absorbed doses. This shows that much smaller arrays can be used to build reliable dosimeter systems, while expected sensitivity could be at the level of 0.1 V/Gy. It is also clear that high repeatability of the array sensors under irradiation allows performing sensitivity enhancement by electronic means. Dense Vm distributions allow new applications, like Gamma imaging and spectroscopy and detection of energetic ions (discussed in Sections 3.4–3.6).

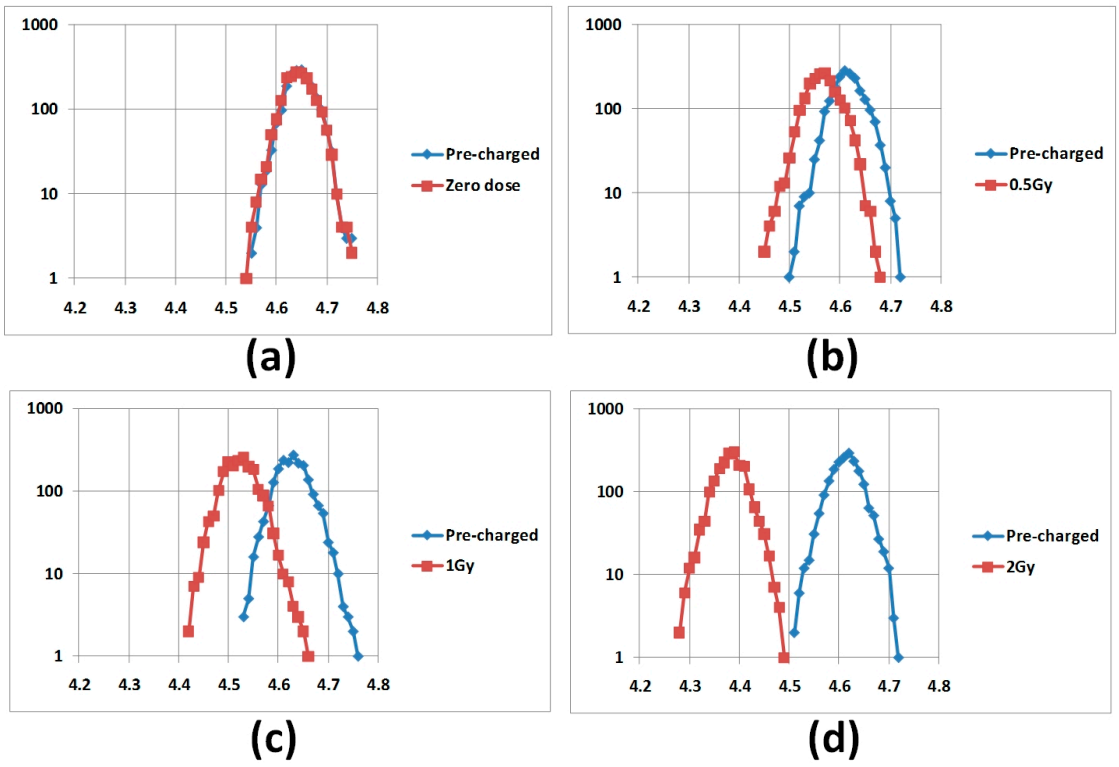

Figure 12. *Cont.*

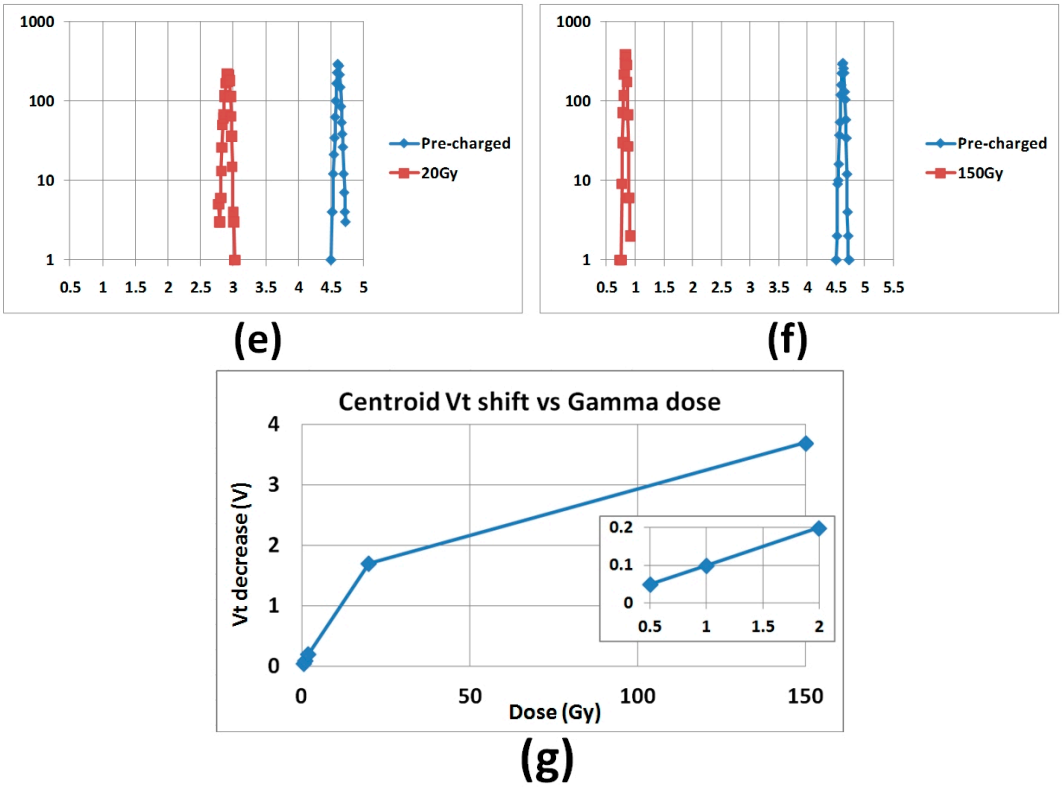

Figure 12. 2k arrays response to Gamma (CLINAC): (**a**–**f**) Vt distributions; (**g**) distributions centroid summary (inset—zoom to small doses). The reference array ("zero dose") was not exposed to radiation.

3.4. Spectral Response

3.4.1. X-ray (100 kVp) vs. Gamma (Co-60) experiment

In this Section, the response to Gamma radiation is compared with the response to X-rays for two types of structures: C-Sensors and STI NMOS transistors.

C-Sensors of three FG geometry types were utilized (Figure 13a). All types of sensors have sensing capacitor of the same area, but different periphery length: type 1—~60 μm, type 2—~95 μm, type 3—~200 μm. All sensors were charged to Vt = ~5 V. Then, sensors were exposed to doses of 10 Gy and 100 Gy. The doses were chosen to investigate sensors response in "linear" and "saturation" stages of discharge. After the irradiations, Vt of all sensors was measured. The results are summarized in Figure 13b.

First, at the "linear" stage of discharge, we see that the response of sensors to X-ray is about 3 times stronger than to Gamma. Second, at the "saturation" stage, the level of final Vt is defined by sensor FG shape, and is not dependent on the type of radiation. Lower Vt level corresponds to longer periphery length of the sensor. This is explained by electrostatic considerations: the N-well (NW) formed between FG "fingers" is kept at 5 V during all read operations. Thus, the potential of the FG is defined by the superposition of NW potential and IPW potential (swept down to −2 V to define the Vt value). Therefore, longer FG periphery leads to higher "fringe" capacitance of FG to NW, thus requiring lower IPW voltage to "close" the readout transistor of the sensor.

The Vt of NMOS transistors having STI as a gate dielectric (Figure 6a of Section 2.2), was measured before and after the exposure to X-ray and Gamma radiation of 10 Gy and 100 Gy doses (Figure 13c). The spread of initial Vt of NMOS transistors is related to the fluctuations of charge trapped in STI dielectric bulk and its interface with Silicon.

For both doses, the response of STI transistors to X-ray was stronger than the response to Gamma. In the case of 10 Gy, the difference was about 3 times, and in the case of 100 Gy, the difference was

about 30%. It is known (and also observed in Section 3.2) that the degradation rate of MOS structures decreases with radiation dose.

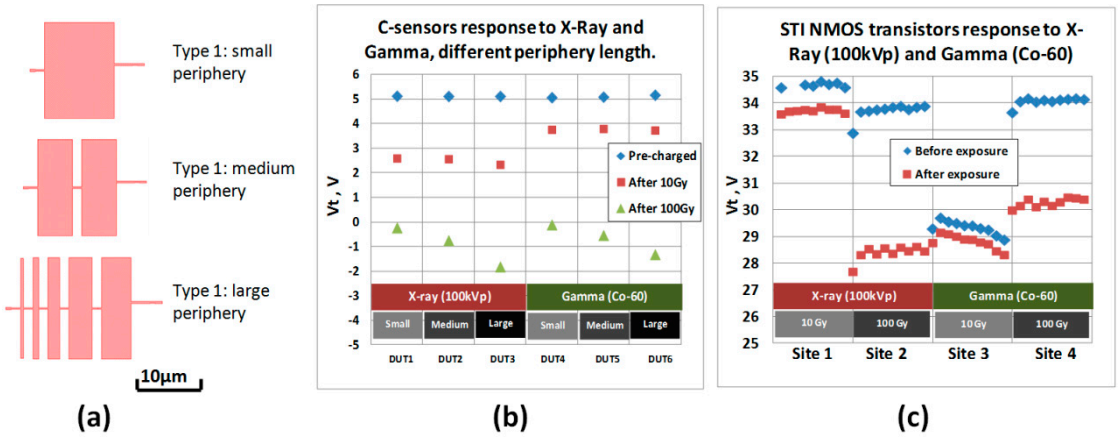

Figure 13. X-ray vs. Gamma experiment: (**a**) sensors FG geometry; (**b**) sensors response; (**c**) NMOS STI transistors response.

In conclusion, for both FG and NMOS structures, we observed stronger response to X-rays than to Gamma radiation. The Vt of charged FG devices under irradiation changes due to charge separation in STI (Section 3.1). The Vt of NMOS devices under irradiation changes due to Boron deactivation (Section 3.2). However, for both (different) mechanisms, X-rays lead to stronger response than Gamma. This observation, actually, indicates that the transfer of the same energy (=dose) from radiation to silicon containing materials corresponds to different amounts of charged particles, depending on both the primary mechanism of interaction (Compton or Photoelectric), as well as secondary energy loss effects.

3.4.2. X-ray Energy Experiment Using 4K Arrays of C-Sensors

In this section, we report on the irradiation experiments with 4K arrays of C-Sensors. All sensors in the fabricated arrays were charged uniformly to Vt about 4 V and exposed to 228 ± 1 mGy dose of X-rays of different energy. After the exposure, the Vt distributions were re-measured (Figure 14a–d), and the Vt distribution centroid shift was calculated for each energy level (Figure 14e).

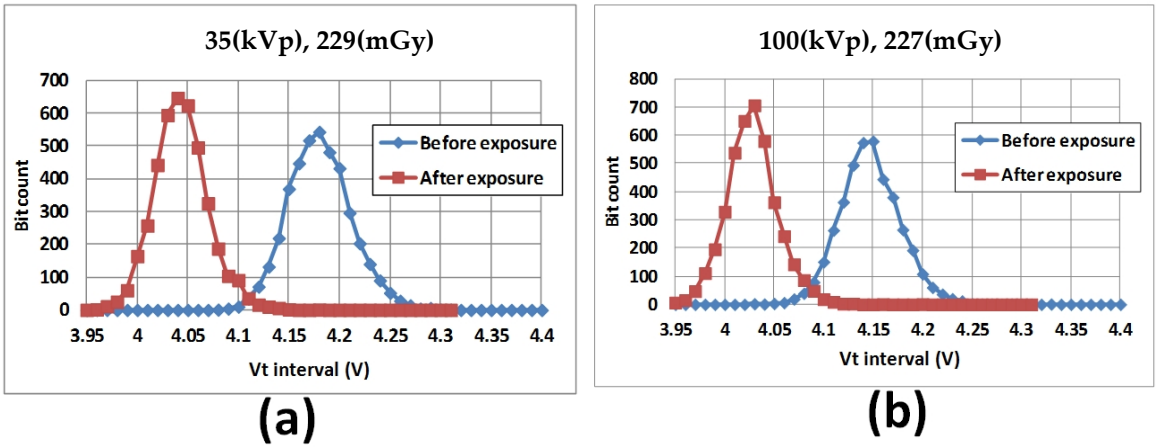

Figure 14. *Cont.*

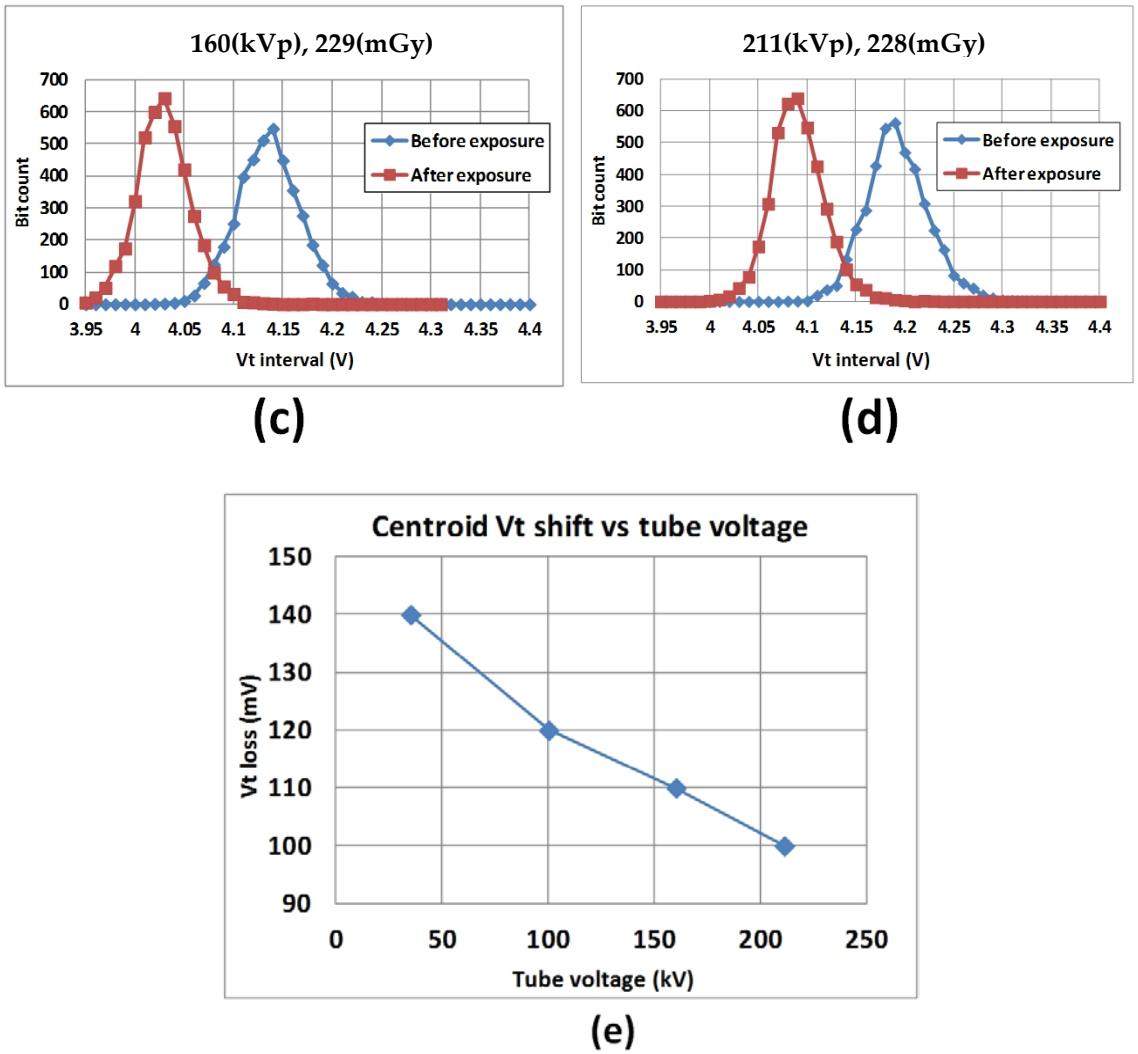

Figure 14. The response of 4K arrays of C-Sensors to X-rays with different energy: (**a**–**d**) Vt distributions before and after irradiation; (**e**) dependence of Vt distribution peak shift on X-ray tube voltage.

A pronounced and strongly repeatable dependence of the sensor response on X-ray photon energy is observed confirming single cell results and demonstrating excellent reproducibility of single C-Sensors.

3.5. Direct Gamma Imaging

Gamma and X-ray imaging is important in different fields of engineering, medicine and security. The imagers are usually based on arrays of photodiodes, covered by scintillator layers. The scintillator converts ionizing radiation into visible light, which is detected by the underlying photodiode array. In order to obtain images of good quality, the photon energy should be high enough to penetrate the material of interest. On the other hand, the efficiency of scintillator decreases at higher photon energies. Thus, X-rays in the range of 50–150 kVp are utilized in most applications. The spatial resolution of an imager is limited by the thickness of scintillator, which is typically about 100 μm [36–38]. The trade-off in scintillator thickness selection is between the strength of the signal and pixel-to-pixel cross-talk. Using thicker scintillator results in more light and improves signal-to-noise ratio in pixels, thus leading to more contrast image. However, it also leads to more light being spread to neighboring pixels (cross-talk), thus reducing the image sharpness. In direct radiation sensors, the cross-talk between pixels is small, and spatial resolution is defined by the pixel size and the size of electron packet, created

by X-ray photon. Thus, using smaller pixels would allow increasing the spatial resolution of imager (when the size of the pixel is still smaller than electron package size; typical pitch of direct radiation imager pixels are 20–100 μm [39]).

In Section 3.3 above, excellent repeatability of sensors arranged in a 2D matrix was demonstrated. Below, we show an ability of the developed array sensor to take images under the ionizing radiation. A small lead particle was glued atop of array region using epoxy resin (Figure 15a) and exposed to Cs-137 radiation source.

The array was uniformly pre-charged to Vt of 4.2V and exposed to the beam of Cs-137 source at a dose rate of 14 mGy/min. The read-out of array was performed at time points of 300 s, 600 s, 900 s, 1500 s and 2100 s. On the acquired Vt distributions (Figure 15c), 2 peaks can be observed, corresponding to uncovered cells (lower Vt) and cells covered with lead (higher Vt). Vt values spread between the peaks corresponds to cells having thinner lead above them (the lead particle has an irregular shape).

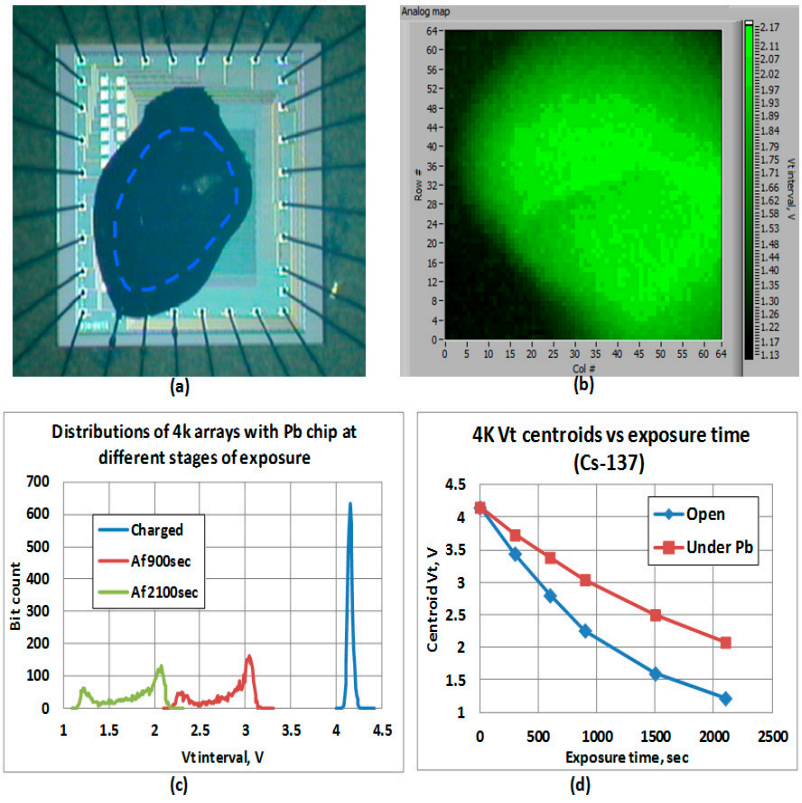

Figure 15. Gamma imaging experiment: (**a**) the chip with C-Sensor array and a lead grain (the large dark stain is epoxy, and inside the epoxy, one can see the lead particle); (**b**) sensor bit-map after the exposure (the particle "image" on the bitmap appears mirrored due to columns address scrambling); (**c**) examples of Vt distributions at different stages of the experiment; (**d**) Vt distribution peaks in the course of irradiation (with and without lead).

3.6. Energetic Ions Detection

Detection of high-energy ions is required in medicine, aerospace applications and various fields of physics research. In this work, it was intended for deeper physical insight into the local processes of charged particle interaction with the solid state.

For the ion bombardment experiment, Oxygen ions with energy of 50 MeV were utilized. According to the performed SRIM simulations, the 50 MeV ion of Oxygen delivers ~120 eV energy per Angstrom thickness in STI of the sensing capacitor. In 3500 A STI, the ion dissipates ~120 × 3500 = 4.2 × 10^5 eV

of energy. The amount of produced e-h pairs in STI is 4.2 × 10^5 eV/17 eV = 25,000 pairs. Since for Vt change of 1 V, it is required to remove 150,000 electrons from the FG, a single ion is expected to result in ~160 mV Vt shift of C-Sensor, making detection of even a single ion feasible.

The doses of ions: 1400, 6500, 13,000, 51,000, 99,000 ions per 100 × 100 μm^2 squares, or 50, 230, 520, 1800, 3500 ions per sensor accordingly were used. The pattern of 100 × 100 μm^2 squares (Figure 16a) was chosen to assure that, on one hand, most of sensor "pixels" would be irradiated uniformly, and, on the other hand, several doses, applied to different location of the same array, would not result in a cross-talk.

As in the case of Gamma, X-ray and UV irradiations, the array sensors were charged uniformly before the exposure (Figure 16b). The twofold Vt distribution after charging corresponds to two types of cells in array: with and w/o M1 shield above the sensing capacitor (different coupling ratios). Two types of cells were used to evaluate the influence of metal routing over the sensor. After the ion bombardment in a passive mode, the Vt distributions were acquired again (Figure 16b).

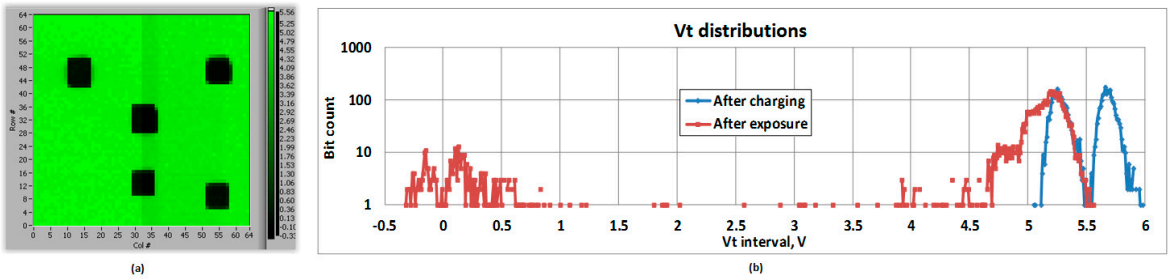

Figure 16. Ion bombardment experiment: (**a**) The Vt pattern after irradiation (dark squares are the 100 μm × 100 μm irradiated areas); (**b**) Vt distributions before and after the exposure.

Figure 16b also shows that a higher (compared with X-rays) sensitivity to ions is observed: the penetration of single ion results in Vt shift of more than 100 mV (close to the predicted 160 mV). ~50 ions result in Vt shift of 5 V (sensor already close to the "saturation" regime). A single ion results in the Vt shift of more than one hundred mV, which corresponds to ~15,000 of electrons removed from the FG.

4. Summary

Novel direct sensors of ionizing radiation, based on floating gate principle ("C-Sensors") were proposed and implemented in a standard 0.18 μm CMOS technology. Compared with the other semiconductor devices (e.g., semiconductor diodes) used for radiation measurements, these sensors use Floating Gate principle (storing of charge in the floating gate and its decrease under irradiation). Floating Gate C-Sensors do not require an energy sources during radiation detection procedure and allow measurements of radiation from sources with the low dose rate (comparable with the background radiation). Charging of the FG is performed by Fowler-Nordheim injection by currents in the nanoAmpere range and with voltages divided between the CG and TG. This allows avoiding using energy consuming high voltage devices in the drivers of practical solutions employing the C-Sensors. Moreover, the sensor readout is performed using a modified CMOS inverter schematics [40], thus allowing ultra-low power operation also in the read-out mode. The mentioned features enable fabrication of ultra-low power consuming integrated dosimeters, suitable for application in RFID systems and other applications with limited energy sources.

Small footprint of the developed C-Sensors allowed implementation of 4k C-Sensor arrays and demonstration of excellent reproducibility of the results from single sensors. The sensitivity in radiation measurement could be increased by averaging the results from individual sensors. Novel applications, such as imaging in high energy ionizing radiation and detection of energetic ions were shown feasible using the designed C-Sensor arrays.

C-Sensors were investigated in depth to reveal the peculiarities of the operation physics and limitations connected with the degradation of the employed materials under radiation. Original methodologies of radiation sensor testing and their reliability assessment were developed and applied to characterize different flavors of the suggested devices and specially fabricated test structures. The obtained results allowed specifying a roadmap for C-sensor improvement. For example, a strong correlation of the degradation immunity with the doping of the sensor electrodes was found. Another direction in further sensor optimization is calibration of STI thickness and finding more efficient device layouts. From the design perspective, practical ultra-low power dosimetry systems based on the suggested approach were demonstrated and are being implemented in medical and consumer applications.

Acknowledgments: The authors wish to thank the following specialists for assistance in irradiations and valuable discussions: Konstantin Lavrenkov and Yaron Leibovich of Soroka Medical Center, Israel; Rafi Srebro of Ben-Gurion University of Negev, Israel; Dmitry Ginzburg of Rotem Industries, Israel; Calogero Pace of University of Calabria, Italy; Felix Palumbo, of CAC-CNEA, Argentina.

Author Contributions: Evgeny Pikhay: Design of experiments and test structures, Acquisition of data, Analysis and interpretation of data, Drafting of manuscript. Yakov Roizin and Yael Nemirovsky: Problem definition, Analyses and interpretation of data, Critical revision of the manuscript.

Conflicts of Interest: The authors declare no conflicts of interest.

References

1. Auricchioa, N.; Carolia, E.; Donatia, A.; Dusib, W.; Fougeresc, P.; Landinia, G. Thin CdTe detectors mounted in back-to-back confguration: Spectroscopic performance for low-energy X- and Gamma-rays. *Radiat. Meas.* **2001**, *33*, 867–872. [CrossRef]
2. Carroll-Ramsey Associates. *Silicon PIN Diode Radiation Detectors*; Carroll-Ramsey Associates: Berkeley, CA, USA, 1999. Available online: http://www.carroll-ramsey.com/detect.htm (accessed on 28 July 2017).
3. Oliveira, F.; Amaral, L.L.; Costa, A.M.; Netto, T.G. In vivo dosimetry with silicon diodes in total body irradiation. *Radiat. Phys. Chem.* **2014**, *95*, 230–232. [CrossRef]
4. Jackson, T.; Fine, L. Dosimeter Charging and/or Reading Apparatus. U.S. Patent 4,224,522, 23 September 1980.
5. Rosenfeld, A.B.; Tavernier, S.; Gektin, A.; Grinyov, B.; Moses, W.W. Semiconductor detectors in radiation medicine: Radiotherapy and related applications. In *Radiation Detectors for Medical Applications*; Springer: New York, NY, USA, 2006; pp. 111–147.
6. Rosenfeld, A.; Holmes-Siedle, A.; Cornelius, I.M. Edge-on Face-to-Face MOSFET for Synchrotron Microbeam Dosimetry: MC modeling. *IEEE Trans. Nucl. Sci.* **2005**, *22*, 2562–2569. [CrossRef]
7. Holmes-Siedle, A.; Adams, L. RADFET: A review of the use of metal-oxide-silicon devices as integrating dosimeters. *Radiat. Phys. Chem.* **1986**, *28*, 235–244. [CrossRef]
8. Sarrabayrouse, G.; Siskos, S. Low dose measurement with thick gate oxide MOSFETs. *Radiat. Phys. Chem.* **2012**, *81*, 339–344. [CrossRef]
9. Hsieh, W.-C.; Lee, H.-T.D.; Jong, F.-C.; Wu, S.-C. Performance Improvement of Total Ionization Dose Radiation Sensor Devices Using Fluorine-Treated MOHOS. *Sensors* **2016**, *16*, 450. [CrossRef] [PubMed]
10. Scheik, L.Z.; McNulty, P.J.; Roth, D.R. Dosimetry based on the erasure of floating gates in the natural radiation environments in space. *IEEE Trans. Nucl. Sci.* **1998**, *45*, 2681–2688. [CrossRef]
11. Fullem, T.Z.; Lehman, L.P.; Cotts, E.J. Examination of the utility of commercial-off-the-shelf memory devices as X-ray detectors. In Proceedings of the 2007 IEEE Nuclear Science Symposium Conference Record, Honolulu, HI, USA, 26 October–3 November 2007.
12. Scheick, L.Z.; McNulty, P.J.; Roth, D.R.; Davis, M.; Mason, B.E. Measurements of dose with individual FAMOS transistors. *IEEE Trans. Nucl. Sci.* **1999**, *46*, 1751–1756. [CrossRef]
13. Roizin, Y.; Aloni, E.; Birman, A.; Dayan, V.; Fenigstein, A.; Nahmad, D.; Pikhay, E.; Zfira, D. C-Flash: An Ultra-Low Power Single Poly Logic NVM. In Proceedings of the 2008 Joint Non-Volatile Semiconductor Memory Workshop and International Conference on Memory Technology and Design, Opio, France, 18–21 May 2008; pp. 90–92.

14. Dagan, H.; Shapira, A.; Teman, A.; Mordakhay, A.; Jameson, S.; Pikhay, E.; Dayan, V.; Roizin, Y.; Socher, E.; Fish, A. A Low-Power Low-Cost 24 GHz RFID Tag With a C-Flash Based Embedded Memory. *IEEE J. Solid-State Circuits* **2014**, *49*, 1942–1957. [CrossRef]
15. Dagan, H.; Teman, A.; Fish, A.; Pikhay, E.; Dayan, V.; Roizin, Y. A Low-Cost Low-Power Non-Volatile Memory for RFID Applications. In Proceedings of the 2012 IEEE International Symposium on Circuits and Systems (ISCAS 2012), Seoul, Korea, 20–23 May 2012.
16. Tarr, N.G.; Mackay, G.F.; Shortt, K.; Thomson, I. A Floating Gate MOSFET Dosimeter Requiring No External Bias Supply. In Proceedings of the Fourth European Conference on Radiation and Its Effects on Components and Systems (RADECS 1997), Cannes, France, 15–19 September 1997.
17. Garcia-Moreno, E.; Picos, R.; Isern, E.; Roca, M.; Font, J.; Suenaga, K. CMOS Current Source Based Radiation Sensors. In Proceedings of the 2010 10th IEEE International Conference on Solid-State and Integrated Circuit Technology (ICSICT 2010), Shanghai, China, 1–4 November 2010.
18. Tarr, N.; Thomson, I. Method of Monitoring Radiation Using a Floating Gate Field Effect Transistior Dosimeter, and Dosimeter for Use Therein. U.S. Patent 6,172,368, 9 January 2001.
19. Arsalan, M.; Shamim, A.; Tarr, N.; Roy, L. Miniaturized, Low Power FGMOSFET Radiation Sensor and Wireless Dosimeter System. U.S. Patent 12/580,670, 27 August 2013.
20. Knoll, M.; Braunig, D. MOS Dosimeter. U.S. Patent 4,788,581, 29 November 1988.
21. Isern, E.; Roca, M.; Garcia-Moreno, E.; Font, J.; Cesari, J.; Pineda, A. Characterization of a floating-gate radiation sensor for X-ray dose detection. In Proceedings of the Radiation and Its Effects on Components and Systems (RADECS 2013), Oxford, UK, 23–27 September 2013.
22. Cesari, J.; Gómez, D.; Roca, M.; Isern, E.; Pineda, A.; García-Moreno, E. Floating Gate P-MOS Radiation Sensor Charging Cycles Characterization. In Proceedings of the IEEE Radiation Effects Data Workshop (REDW 2014), Paris, France, 14–18 July 2014.
23. Wang, Y.; Tatv, G.; Wang, Y. A Novel Fully Integrated Floating-Gate MOSFET Radiation Dosimeter Using VTH Extractor. In Proceedings of the 2nd Annual IEEE Northeast Workshop on Circuits and Systems (NEWCAS 2004), Montreal, QC, Canada, 20–23 June 2004.
24. Martin, M.N.; Roth, D.R.; Garrison-Darrin, A.; McNulty, P.J.; Andreou, A.G. FGMOS dosimetry: Design and implementation. *IEEE Trans. Nucl. Sci.* **2002**, *48*, 2050–2055. [CrossRef]
25. Tarr, N.G.; Shortt, K.; Wang, Y.; Thomson, I. A Sensitive, Temperature-Compensated, Zero-Bias Floating Gate MOSFET Dosimeter. *IEEE Trans. Nucl. Sci.* **2004**, *51*, 1277–1282. [CrossRef]
26. Braunig, D.; Wulf, F. Atomic displacement and total ionizing dose damage in semiconductors. *Radiat. Phys. Chem.* **1994**, *43*, 105–127. [CrossRef]
27. Benedetto, J.; Hughes, H.L. Radiation Effects and Hardening of MOS Technology: Devices and Circuits. *IEEE Trans. Nucl. Sci.* **2003**, *50*, 500–521.
28. Snyder, E.S.; McWhorter, P.J.; Dellin, T.A.; Sweetrnant, J.D. Radiation response of floating gate EEPROM memory cells. *IEEE Trans. Nucl. Sci.* **1989**, *36*, 2131–2139. [CrossRef]
29. McNulty, P.J.; Yow, S.; Scheick, L.Z.; Abdel-Kader, W.G. Charge Removal From FGMOS Floating Gates. *IEEE Trans. Nucl. Sci.* **2002**, *49*, 3016–3021. [CrossRef]
30. Bagatin, M.; Gerardin, S.; Cellere, G.; Paccagnella, A.; Visconti, A.; Bonanomi, M.; Beltrami, S. Error Instability in Floating Gate Flash Memories Exposed to TID. *IEEE Trans. Nucl. Sci.* **2009**, *56*, 3267–3273. [CrossRef]
31. Naumova, O.V.; Fomin, B.I.; Ilnitsky, M.A.; Popov, V.P. Charge accumulation in the buried oxide of SOI structures with the bonded Si/SiO_2 interface under γ-irradiation: Effect of preliminary ion implantation. *Semicond. Sci. Technol.* **2012**, *27*, 065014. [CrossRef]
32. Brown, D.B.; Saks, N.S. Time dependence of radiation-induced interface trap formation in metal-oxide-semiconductor devices as a function of oxide thickness and applied field. *J. Appl. Phys.* **1991**, *70*, 3734–3747. [CrossRef]
33. Katznelson, R.; Frohman-Bentchkovsky, D. An Erase Model for FAMOS EPROM Devices. *IEEE Trans. Electron Devices* **1980**, *27*, 1744–1752. [CrossRef]
34. Jafari, H.; Feghhi, S.; Boorboor, S. The effect of interface trapped charge on threshold voltage shift estimation for gamma irradiated MOS device. *Radiat. Meas.* **2015**, *73*, 69–77. [CrossRef]
35. Witczak, S.C.; Lacoe, R.C.; Mayer, D.C.; Fleetwood, D.M.; Schrimpf, R.; Galloway, K.F. Space Charge Limited Degradation of Bipollar Oxides at Low Electric Fields. *IEEE Trans. Nucl. Sci.* **1998**, *45*, 2339–2351. [CrossRef]

36. Miyata, B.; Tawa, N.; Mukai, K.; Tsunemi, H.; Miyaguchi, K. High Resolution X-ray Photon-Counting Detector with Scintillator-deposited Charge-coupled Device. In Proceedings of the IEEE Nuclear Science Symposium Conference Record, Rome, Italy, 16–22 October 2004.
37. Cha, A.K.; Kim, B.-J.; Cho, G.; Jeon, S.C.; Bae, J.H.; Chi, Y.K.; Lim, G.-H.; Kim, Y.-H. A Pixelated CsI (Tl) Scintillator for CMOS-based X-ray Image Sensor. In Proceedings of the IEEE Nuclear Science Symposium Conference, San Diego, CA, USA, 29 October–1 November 2006.
38. Spartiotis, K.; Durrant, R.; Leppänen, A.; Lohman, H.; Männistö, O.; Pantsar, T.; Pyyhtiä, J.; Schulman, T. X- and Gamma ray Imaging Systems based on CdTe-CMOS Detector Technology. In Proceedings of the IEEE Nuclear Science Symposium Conference Record, Dresden, Germany, 19–25 October 2008.
39. Dupont, B.; Dierickx, B.; Ahmed, N. Photon Counting and Color X-ray Imaging in Standard cis Technology. Available online: http://www.caeleste.com/caeleste_publications/Caeleste_photon_counting_color_xray_web.pdf (accessed on 28 July 2017).
40. Audzeyeu, M.; Makarevich, Y.; Shvedau, S.; Belous, A.; Pikhay, E.; Dayan, V.; Roizin, Y. Floating Gate Inverter Type Memory Cell and Array. U.S. Patent 8,378,407, 24 June 2010.